Electronic structure and magneto-optical Kerr effect of Fe_3O_4 and Mg^{2+}- or Al^{3+}-substituted Fe_3O_4

V. N. Antonov,* B. N. Harmon, and V. P. Antropov
Ames Laboratory, Iowa State University, Ames, Iowa 50011

A. Ya. Perlov and A. N. Yaresko
Max Planck Institute for Physics of Complex Systems, D-01187 Dresden, Germany

(Received 7 October 1999; revised manuscript received 25 April 2001; published 5 September 2001)

The optical and magneto-optical spectra of charge-ordered magnetite (Fe_3O_4) below the Verwey transition and Mg^{2+}- and Al^{3+}-substituted Fe_3O_4 are investigated theoretically from first principles, using the fully relativistic Dirac linear muffin-tin orbital band structure method. The electronic structure is obtained with the local spin-density approximation (LSDA), as well as with the so-called LSDA+U approach for which the charge ordering is found to be a stable solution with an energy gap value of 0.19 eV (the experimental value is 0.14 eV) in contrast to a metallic state given by LSDA. The origin of the Kerr rotation realized in the compounds is examined.

DOI: 10.1103/PhysRevB.64.134410 PACS number(s): 75.30.Mb, 71.28.+d, 71.20.−b

I. INTRODUCTION

The metal-insulation transition (MIT) has fascinated theorists and experimentalists for many years. This transition is associated with Sir N. Mott who laid down the foundations for physical understanding of this phenomenon.[1] One of the most famous MIT compounds is magnetite Fe_3O_4 which exhibits the so-called Verwey metal-insulation transition.[2]

Historically, magnetite, discovered before 1500 B.C., is the first known magnet and is extensively used for industrial applications, notably in magnetic recording. Most of the properties of magnetite have been thoroughly studied and are well documented.[3,4] However, the electronic structure of Fe_3O_4 as well as that of many other MIT compounds is still a subject of debate.[5]

Fe_3O_4 is a strongly correlated $3d$ compound which is ferrimagnetically ordered below a high transition temperature ($\sim$850 K). The valence of various atoms is described by the formal chemical formula, $Fe_A^{3+}[Fe^{2+}Fe^{3+}]_B(O^{2-})_4$. The tetrahedral lattice sites (A sites) in the inverse spinel structure are occupied by Fe^{3+} ions, whereas the octahedral lattice sites (B sites) are occupied alternately by equal numbers of Fe^{2+} and Fe^{3+}. At $T_V=120$ K Fe_3O_4 undergoes a first-order phase transition (Verwey transition).[2] This is a particular MIT that has been studied for quite some time.[6] The Verwey transition is characterized by an abrupt increase in the electrical conductivity by two orders of magnitude on heating through T_V.[7] Verwey and co-workers[2,8] were the first to point out that this transition is associated with an electron localization-delocalization transition. The Fe^{2+} ion can be regarded as an ''extra'' electron plus an Fe^{3+} ion. When all B sites are equivalent, the ''extra'' electron is moving between Fe_B^{3+} ions and the system is a mixed valent metal, with average Fe_B valence, $Z=2.5$. The Verwey phase transition below T_V is accompanied by long-range charge ordering (LRCO) of Fe^{3+} and Fe^{2+} ions on $B1$ and $B2$ sites of the B sublattice. Indeed, studies by electron and neutron diffraction and nuclear magnetic resonance[9–11] show that below T_V the $B1$ and $B2$ sites are structurally distinguishable with the crystal structure slightly distorted because of the charge ordering. Just how these charges arrange themselves has been the subject of debate[6] since Verwey first proposed that, below T_V, all Fe_B^{3+} and Fe_B^{2+} sit on different chains.[2]

The electronic structure of Fe_3O_4 has been investigated experimentally by means of soft x-ray spectroscopy,[12–14] Seebeck-effect measurements,[15] photoelectron spectroscopy,[16–22] optical,[23,24] and magneto-optical[25–29] (MO) spectroscopies, and by magnetic dichroism.[30,31] The optical data[24] indicate a gap of 0.14 eV between occupied and empty electronic states and show also a strong temperature dependence of the optical conductivity in the energy region of 0–1 eV.

The interpretation of the optical and MO spectra of Fe_3O_4 is very difficult due to the existence of three kinds of iron atoms, i.e., Fe_B^{2+}, Fe_B^{3+}, and Fe_A^{3+}. The substitution for one of the types of iron ions by nonmagnetic ions provides a possibility for distinguishing transitions from various sites. There are several such experimental studies in the literature. Simsa and co-workers reported the polar Kerr rotation and ellipticity of Fe_3O_4 as well as the influence of a systematic substitution of Fe^{2+} by Mn^{2+} in the 0.5–3.0 eV energy range.[27] Zhang and co-workers reported the polar Kerr spectra and the off-diagonal element of the dielectric tensor of Fe_3O_4 between 0.5 and 4.3 eV. They also reported spectra of $Li_{0.5}Fe_{2.5}O_4$ and $MgFe_2O_4$ between 0.5 and 5.0 eV.[25] Finally, recent investigation of the optical and MO spectra of Fe_3O_4, Al^{3+}, and Mg^{2+} substitution has been carried out in Ref. 26. The measurements were performed for the high-temperature metallic phase of Fe_3O_4. The authors systematically study the influence on the MO-Kerr spectrum of Fe_3O_4 by partial substitution of Fe^{2+} by Mg^{2+} and of Fe^{3+} by Al^{3+}, with the concentration of the substituent as a parameter. As a result the authors were able to establish the nature of the MO-active transitions by investigation of relative intensities of main peaks in the off-diagonal optical conductivity of the Mg and Al substituted compounds.

Energy band-structure calculations for Fe_3O_4 in the high-temperature cubic phase have been presented in Ref. 32 us-

ing the self-consistent spin-polarized augmented plane-wave (APW) method with the local spin-density approximation. The calculations show that Fe_3O_4 is a half metallic ferrimagnet. The Fermi level crosses only the minority spin energy bands consisting of t_{2g} orbitals on the Fe(B) sublattice. There is an energy gap for the majority spin bands at the Fermi level. A similar energy-band structure of Fe_3O_4 was obtained in Ref. 33 using the linear muffin-tin orbital (LMTO) method. The authors estimated the hopping integrals and the electron interaction parameters entering a model Hamiltonian for the motion of the ''extra'' electrons on the B sublattice using the ''constrained'' density-functional theory. It was found that the on-site Coulomb interaction parameter for the Fe(B) site is equal to 4.1 ± 0.5 eV. Both the local spin-density approximation (LSDA) band-structure calculations gave only a metallic solution without charge ordering with partially filled bands (containing one electron per two B sites). The energy-band structure for charge ordering in the low-temperature phase of Fe_3O_4 has been calculated in Ref. 34 using the LMTO method in the LSDA$+U$ approximation. The charge ordering was found to be a semiconducting state with an energy gap value of 0.34 eV. Since the LSDA$+U$ results do yield a gap, it is of interest to investigate other properties to determine the overall applicability of the approach. To this end one may compare the theoretically calculated and experimentally measured optical and MO spectra, providing information on both the occupied and empty states. This is particularly important for determination of energy positions of the upper and lower Hubbard bands of strongly correlated Fe d states in magnetite.

Details concerning the mechanism of the Verwey transition and the type of LRCO are still unclear. Many elaborate theories for the Verwey transition have been proposed. Anderson[35] pointed out the essential role of short-range charge ordering (SRCO) in the thermodynamics of the transition. The observed entropy change in the transition [($\sim$0.3 to 0.35) R/B-site mole] is decisively smaller than the $R \ln 2 = 0.69R$ expected in a complete order-disorder transition. Anderson interpreted the Verwey transition as a loss of the LRCO of the ''extra'' electrons on the B sublattice at temperatures above T_V while the short-range charge order is maintained across the transition. Using a Hartree-Fock analysis, Cullen and Callen[36] showed that an ordering transition could occur in Fe_3O_4 as a function of the ratio V/B, where B is the bandwidth of the ''extra'' electrons in the absence of disorder. The transition in this case is of second order, while experimentally a first-order transition is observed. The conduction mechanisms in Fe_3O_4 have been reviewed by Mott[37] (see also Refs. 6 and 38).

One of the fundamental questions concerning the Verwey transition in Fe_3O_4 is whether the 3d states are localized or itinerant. This question is most frequently answered by comparison between experimental spectroscopies and the different theoretical descriptions. Optical and MO spectroscopy, like photoelectrons spectroscopy and bremsstrahlung isochromat spectroscopy, supply direct information about the energy states (both occupied and unoccupied) in a wide energy interval around the Fermi energy, and can provide means of discrimination between the different theoretical limits.

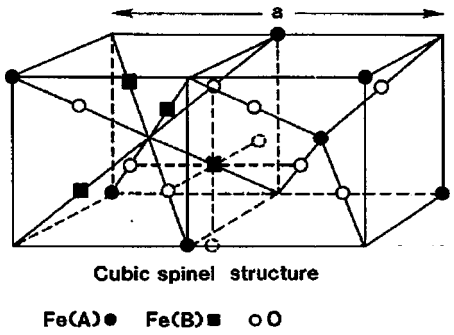

FIG. 1. Crystal structure of Fe_3O_4.

A basic problem concerning magnetite is that both the localization of the valence states and the mixing of the oxygen p states and iron d states are considerable. The aim of this paper is to present a detailed theoretical study of the electronic structure, optical, and MO properties of Fe_3O_4 in the low-temperature phase within the band-structure approach which takes strong correlations into account. This is achieved by applying a local spin-density approximation to the density-functional theory supplemented by a Hubbard U term (LSDA$+U$). We also calculated the electronic structure of the Mg^{2+}- and Al^{3+}-substituted Fe_3O_4 compounds. Our study motivated by the fact that although a large number of investigations have been devoted to the experimental study of the optical and MO spectra of Fe_3O_4,[25–29] to our best knowledge there are no first-principles calculations of the optical and magneto-optical properties of magnetite Fe_3O_4 as well as Mg^{2+}- and Al^{3+}-substituted Fe_3O_4.

The paper is organized as follows. Section II presents a description of the crystal structure of the Fe_3O_4 compound and the computational details. Section III is devoted to the electronic structure, optical, and MO properties of the Fe_3O_4 and Mg^{2+}- and Al^{3+}-substituted Fe_3O_4 calculated in the LSDA and LSDA$+U$ approximations. The optical and MO theoretical calculations are compared to the experimental measurements. Finally, the results are summarized in Sec. IV.

II. CRYSTAL STRUCTURE AND COMPUTATIONAL DETAILS

Fe_3O_4 crystallizes in the face-centered-cubic (fcc) inverse spinel structure (Fig. 1) with two formula units (14 atoms) per primitive cell. The space group is $Fd\bar{3}m$ (no. 227). The oxygen atoms form a close-packed face-centered-cubic structure with the iron atoms occupying the interstitial positions. There are two types of interstitial sites both occupied by the iron atoms. One site is called the A or 8a site, tetrahedrally coordinated by four O^{2-} ions composing a diamond lattice. The interstices of these coordination tetrahedra are too small for larger Fe^{2+} ions and this site is occupied only by Fe^{3+} ions. Another cation site is called the B or 16d site, and is coordinated by six O^{2-} ions forming slightly distorted octahedra, which line up along the $\langle 110 \rangle$ axes of the cubic lattice sharing edges. The point symmetry of the B site is $D3d$. This site forms exactly one half of a face-centered-cubic lattice.

The lattice of the B site can be considered as a diamond lattice of cation tetrahedra, sharing corners with each other. All the tetrahedra on the same (e.g., xy) plane are isolated. In the following, we refer to $b1$ axes or $b1$ chains and $b2$ axes or $b2$ chains. The $b1$ direction is $[1\bar{1}0]$, $b2$ is [110], and the c axis is [001]. All the Fe octahedral or B sites lie on either $b1$ or $b2$ chains. We also should mention that the distances Fe_A-O_1 and Fe_B-O_2 are different and equal to 1.876 and 2.066 Å, respectively.

In the disordered high-temperature phase the B sites are occupied by equal numbers of Fe^{2+} and Fe^{3+} ions randomly distributed between $B1$ and $B2$ sites. Below T_V the system undergoes a first-order transition accompanied by long-range charge ordering of Fe^{3+} and Fe^{2+} ions on the B sites. Verwey from the very beginning proposed a rather simple charge separation: $b1$ chains occupied only by Fe^{2+} ions and $b2$ chains by Fe^{3+} ions (or vice versa).[2] Since that time the type of charge ordering has been the subject of debate.[6] As an example, in Mizoguchi's model[39] ions run in pairs of Fe^{2+} followed by Fe^{3+} along each b chain. Another charge ordering considers three Fe^{2+} alternating with one Fe^{3+} on one-half of the chains, and a sequence of three Fe^{3+} alternating with one Fe^{2+} on the other half and so on.[6] Despite the wealth of effort devoted to investigating the low-temperature phase of magnetite, there is still no completely satisfactory description of the ordering of the Fe atoms on the octahedral or B sites in this spinel structure. In addition, some experimental measurements show that below the Verwey transition temperature there is a small change in the crystal structure which becomes monoclinic accompanied by a doubling of the unit cell along the a, b, and c axes.[40,41]

In our band-structure calculations we used the experimentally measured constant ($a=8.396$ Å).[42] The details of the computational method are described in our previous papers,[43,44] and here we only mention several aspects. The electronic structure of the compounds was calculated self-consistently using the local spin-density approximation[45] and the fully relativistic spin-polarized LMTO method[46–49] in the atomic-sphere approximation, including the combined correction (ASA+CC).[46,50] The combined correction terms have been included also in calculation of the optical matrix elements.[51] We have calculated the absorptive part of the optical conductivity in a wide energy range. The Kramers-Kronig transformation has been used to calculate the dispersive parts of the optical conductivity from the absorptive parts.

To improve the potential we include two additional empty spheres in the 16c and 48f positions. The radii of the overlapping spheres were $S_{FeA}=2.3293$, $S_{FeB}=2.7524$, $S_O=1.8482$, $S_{E1}=1.7187$, and $S_{E2}=1.6993$ a.u. In our band-structure calculations we neglect the small monoclinic distortion for simplicity. We also adopted the simplest type of charge ordering below T_V initially proposed by Verwey,[2] namely we assume that all the Fe_B^{2+} ions sit on $b1$ chains and all the Fe_B^{3+} on $b2$ chains. The basis consisted of the Fe s, p, d, and f; O, s, p, and d, and empty sphere s, and p LMTO's. The **k**-space integrations were performed with the improved tetrahedron method.[52]

We have adopted the LSDA+U method[53] as a different level of approximation to treat the electron-electron correlation. Usually, the Hubbard-like $U_{\rm eff}$ is evaluated by comparison of theoretically calculated energy positions of energy bands with x-ray photoemission spectroscopy (XPS) and ultraviolet photoemission spectroscopy (UPS) measurements. It can be also evaluated from atomic Dirac-Hartree-Fock (DHF) calculations,[57] Green-function impurity calculations,[58] and from band-structure calculations in the super cell approximation.[59] In our particular case we have two types of Fe ions with different occupation numbers for their 3d shell. Obviously, the effective repulsion of 3d electrons described by $U_{\rm eff}$ depends on the number of holes in the 3d shell (the ionicity), and $U_{\rm eff}$ should increase with increasing ionicity.[60] The estimation in Ref. 33 gave the value of the on-site Coulomb interaction parameter for the Fe(B) site equal to 4.1 ± 0.5 eV. Constrained calculations[34] with two types of charge ordering gave $U_{\rm eff}=4.5$ eV. The calculated value of $U_{\rm eff}$ depends on theoretical approximations and for our purposes it is sufficient to regard the value of $U_{\rm eff}$ as a parameter and try to ascertain its value from comparison of the calculated physical properties of Fe_3O_4 with experiments. We found, however, that the optical and MO spectra are rather insensitive to the precise value of $U_{\rm eff}$. The LSDA+U band-structure calculations with $U_{\rm eff}$ varying from 4 to 6 eV provide optical and MO spectra in a reasonable agreement with the experimental data. On the other hand, the value of the energy gap strongly depends on the value of $U_{\rm eff}$. We set $U_{\rm eff}$ to 4.0 and 4.5 eV for Fe^{2+} and Fe^{3+} ions, respectively. These values give a band gap of 0.19 eV.

III. RESULTS AND DISCUSSION

A. Fe_3O_4

Figure 2 shows the partial density of states obtained from the LSDA calculation. These results agree well with previous band-structure calculations.[32,33] The occupied part of the valence band can be subdivided into several regions separated by energy gaps. The oxygen 2s bands, which are not shown in the figure, appear between -20.0 and -19.7 eV for both spins with the exchange splitting of about 0.2 eV. The next group of bands in the energy region -7.4 to -3.4 eV is formed mostly by oxygen 2p states. The Fed energy bands are located above and below E_F at about -4.0 to 3.0 eV. As indicated from Fig. 2, the exchange splitting between the spin-up and -down d electrons on the Fe atom is about 3.5 eV. In addition to the exchange splitting, the five d levels of the Fe atom are split due to the crystal field. At the A site (T_d point symmetry) in the spinel structure the crystal field causes the d orbitals to split into a dublet e ($3z^2-1$ and x^2-y^2) and a triplet t_2 (xy, yz, and xz). The octahedral component of the crystal field at the B site is strong enough that the t_{2g} (xy, yz, and xz) and e_g ($3z^2-1$ and x^2-y^2) orbitals form two separate nonoverlapping bands. At the B site the crystal field is trigonal ($D3d$), as a result the t_{2g} orbitals split into singlet a_{1g} and doublet e_g'. However, the $a_{1g}-e_g'$ splitting of the t_{2g} band is negligible in comparison with its width in

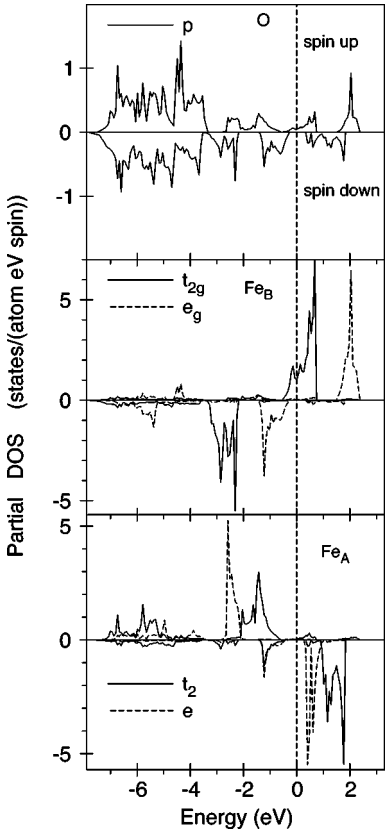

FIG. 2. LSDA partial DOS of Fe_3O_4.

LSDA calculations, therefore in the following we will denote the states formed by a_{1g} and e_g' orbitals as t_{2g} states. Accordingly, we present in Fig. 2 density of states (DOS) of "t_{2g}" orbitals as a sum of the a_{1g} and e_g' ones. The crystal-field splitting Δ_{CF} is approximately 2 eV for the Fe_B atom and 1 eV for the Fe_A atom. This difference may be attributed to the large covalent mixing of the Fe_B orbitals with its six nearest neighbors of the same kind. The spin-polarized calculations show that Fe_3O_4 in the high-temperature phase is a half metallic ferrimagnet. The Fermi level crosses only the majority spin energy bands, consisting of spin-up t_{2g} orbitals on the Fe_B sublattice (Fig. 2). There is an energy gap for the minority spin bands at the Fermi level. Spin-orbit splitting of the d energy band at Γ is about 0.02 eV and much smaller than the crystal-field splitting.

In Fe_3O_4 the magnetic moments within the A and the B sublattices are ferromagnetically aligned while the two sublattices are antiferromagnetic with respect to each other. This magnetic structure was first proposed by Néel[54] to explain the magnetization data and was later confirmed by neutron-scattering measurements.[55] The calculated spin and orbital magnetic moments on various atoms are given in Table I and compared with previous calculations[33] and experimental data.[56] Measurements indicated that the magnetic moment of an iron atom on the A site is much smaller than the $5.0\mu_B$ of a pure Fe^{3+} ion.[56] This is an indication of strong hybridization between the $3d$ orbitals of Fe_A. The orbital magnetic moment is rather small for all the atoms due to small spin-orbit coupling (see Table I).

TABLE I. The experimental and LSDA calculated spin and orbital magnetic moments (in μ_B) of Fe_3O_4. The experimental data are from Ref. 56.

Atom	Ref. 33	M_s	M_l	M_{total}	Expt.
Fe(A)	3.46	3.496	0.025	3.521	3.82
Fe(B)	−3.57	−3.658	−0.043	−3.701	
O	−0.10	−0.052	0.0	−0.052	
E_{sphere}	0.01	0.007	0.0	0.007	
Total	−3.99	−3.965	−0.061	−4.026	−4.1

The application of LSDA calculations to Fe_3O_4 is problematic, because of the correlated nature of d electron in this compound. The intersite Coulomb correlation is well described by the LSDA. However, the on-site Coulomb interaction, which is a driving force for Mott-Hubbard localization, is not well treated within LSDA. As a result, LSDA gives only a metallic solution without charge ordering. To take into account the strong on-site d-d electron-electron correlations we used the LSDA$+U$ method.[53] We started from a $d^5(t_{2\uparrow}^3 e_{\uparrow}^2)$ configuration for Fe_A^{3+} ions on the tetrahedral site of the sublattice A and $d^6(t_{2g\downarrow}^3 e_{g\downarrow}^2 a_{1g\uparrow}^1)$ and $d^5(t_{2g\downarrow}^3 e_{g\downarrow}^2)$ for Fe_B^{2+} and Fe_B^{3+} ions on octahedral site of the sublattices B_1 and B_2, respectively. U_{eff} was applied to all the d states and the occupation numbers were obtained as a result of the self-consistent relaxation. Figures 3 and 4 show the energy-band structure along the symmetry lines and the total and partial density of states obtained from the LSDA $+U$ calculation. In contrast to LSDA, where the stable solution is a metal with a uniform distribution of the $t_{2g\uparrow}$ electrons on the B octahedral sites, the LSDA$+U$ gives a charge-ordered insulator with a direct energy gap value of 0.19 eV at the Γ point. The experimental optical

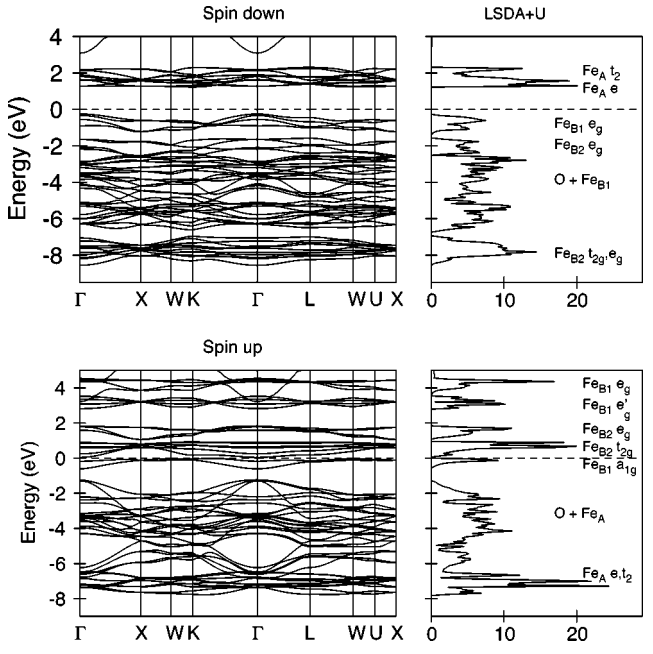

FIG. 3. LSDA$+U$ energy-band structure and total DOS [in states/(unit cell eV)] of Fe_3O_4.

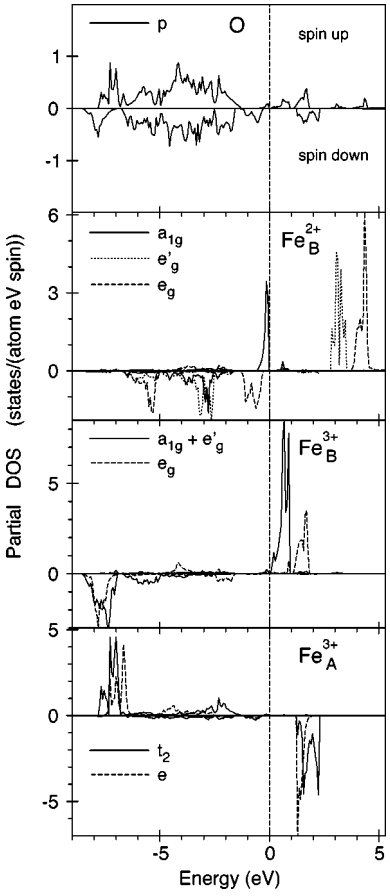

FIG. 4. LSDA+U partial DOS of Fe_3O_4.

measurements[24] gave a gap of 0.14 eV at $T=10$ K. The energy gap occurs between the $Fe_B^{2+}a_{1g\uparrow}$ (the top of valence band) and $Fe_B^{3+}t_{2g\uparrow}$ (bottom of empty conduction band) states (Fig. 4). Actually, our LSDA+U band-structure calculations support the key assumption that Cullen and Callen have made earlier[36] in proposing the one-band model Hamiltonian, where it was assumed that the ''extra'' electron moves in the a_{1g} band split off below the rest of the d bands of other symmetries. Two electrons at the $Fe_B^{2+}a_{1g}$ orbitals situated in the close vicinity of the Fermi level are mostly localized. Other electrons at the $B1$ site are well hybridized with oxygen p electrons (Fig. 4). We should mention that the screening of the Coulomb interaction in Fe_3O_4 is very effective and the system is close to the metallic state. Even a small change in the ratio $(Fe^{2+}/Fe^{3+})_{oct}$, (which we modeled by changing of the occupation numbers of the a_{1g} orbital at the B_1 and B_2 sites in the frame of the ''virtual crystal approximation'' [61]) leads to the closing of the energy gap and a suppression of the metal-insulating transition.[62]

The LSDA+U calculations also improved the agreement between the theoretically calculated and experimental value of the magnetic moment on the A site in comparison with LSDA calculations (see Tables I and II). Although neutron diffraction found that magnetic superstructure scattering in the low-temperature phase of Fe_3O_4 is too weak to be accounted for by an ordering of Fe^{2+} and Fe^{3+} on the B sites, the experimental study did show larger covalency for the

TABLE II. The LSDA+U calculated spin and orbital magnetic moments (in μ_B) of Fe_3O_4.

Atom	M_s	M_l	M_{total}	Expt.
Fe_A^{3+}	3.845	0.018	3.863	3.82
Fe_B^{2+}	−3.541	−0.024	−3.565	
Fe_B^{3+}	−4.002	−0.024	−4.026	
O_1	−0.091	−0.001	−0.092	
O_2	−0.010	0.001	−0.009	
E_{sphere}	0.003	0.0	0.003	
Total	−3.796	−0.003	−3.826	−4.1

Fe^{3+} ions on tetrahedral A sites than those on octahedral B sites.[9] In agreement with such an experimental observation the LSDA+U calculated magnetic moments of Fe^{3+} atoms are equal to 3.845 and $-4.002\mu_B$ for A and B sites, respectively. This can be explained by different nearest-neighbor distances Fe_A-O_1 and Fe_B-O_2.

After the consideration of the above band-structure properties we turn to the optical and MO spectra. In Fig. 5 experimental[23] optical reflectivity and the diagonal part of the dielectric function ε_{xx} of Fe_3O_4 are compared to the theoretical ones calculated within the LSDA and LSDA+U approaches. Better agreement between the theory and the experiment was found when we used the LSDA+U approximation. As was mentioned above, the LSDA theory produces the metallic solution and therefore gives a wrong asymptotic behavior for the optical reflectivity and the dispersive part of the dielectric function ϵ_{1xx} as $\omega\rightarrow 0$. In Fig. 6 we show the calculated and experimental[23,24] absorptive part of the diagonal optical conductivity spectra σ_{1xx} in a wide energy range. The characteristic features of the LSDA calculations of σ_{1xx} is an erroneous peak at 1.9 eV which is absent in the experimental measurements. The absence of this peak in the experiment indicates that the LSDA calculations produce incorrect energy-band positions. Accounting for the Coulomb repulsion U_{eff} strongly influences not only the electronic structure but also the calculated optical spectra of Fe_3O_4. The LSDA+U calculations give reasonably good agreement between the theoretical and the experimental optical spectra of Fe_3O_4 (see Figs. 5 and 6). The calculated optical conductivity spectrum (Fig. 6) can be sorted into the following groups of interband transition: (i) the interband transitions between the Fe $3d$ bands below 2.5 eV, (ii) the transitions from O $2p$ to Fe $3d$ bands in the region of 2.5–9 eV, and (3) Fe $3d\rightarrow 4p$ and O $2p\rightarrow$Fe$4s$ interband transitions above 9 eV. To avoid misunderstanding, we should mention that here and in the following when talking about $d\rightarrow d$ transitions we mean that the energy bands involved in the transitions have predominantly d character, however, the contribution of p or f states to these bands is sufficient to provide a significant transition probability through optical dipole matrix elements.

To explain the microscopic origin of the optical and MO properties of Fe_3O_4 in terms of individual electronic transitions, we performed the decomposition of the calculated σ_{1xx} spectrum into the contributions arising from separate inter-

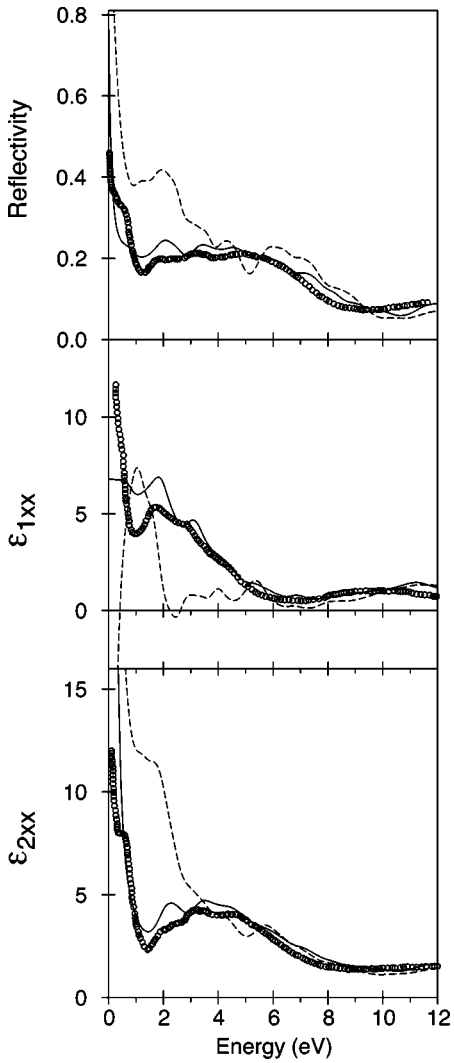

FIG. 5. Optical reflectivity and diagonal parts of the dielectric function ε_{xx} of Fe_3O_4 calculated in LSDA (dashed line) and LSDA$+U$ (solid line) approximation compared with experimental data (Ref. 23) (open circles).

band transitions. It can be done because the energy bands formed by the orbitals of different symmetries belonging to in-equivalent Fe atoms are well separated in energy (see Fig. 3). As one can see in Fig. 7, the first peak situated at 0.9 eV originates from the $Fe_B^{2+}(a_{1g\uparrow}) \rightarrow Fe_B^{3+}(t_{2g\uparrow})$ interband transitions. The next feature at 1.9 eV comes from the $Fe_B^{2+}(a_{1g\uparrow}) \rightarrow Fe_B^{3+}(e_{g\uparrow})$ interband transitions. Peak 3 arises from the $Fe_B^{2+}(e_{g\downarrow}) \rightarrow Fe_A^{3+}(e_{\downarrow}, t_{2\downarrow})$ transitions. Peaks 4, 6, 7, and 8 are mostly determined by O $2p \rightarrow$ Fe $3d$ transitions although Fe $3d \rightarrow$ Fe $3d$ transitions are also involved. The shoulder situated at 3.2 eV originates from the $Fe_B^{3+}(e_{g\downarrow}) \rightarrow Fe_A^{3+}(e_{\downarrow}, t_{2\downarrow})$ interband transitions (peak 5).

Overall, the experimental features are reasonably well reproduced in the LSDA$+U$ calculations, except for the energy shift towards smaller energies of peak 3 in the theoretically calculated optical conductivity responsible for the $Fe_B^{2+}(e_{g\downarrow}) \rightarrow Fe_A^{3+}(e_{\downarrow}, t_{2\downarrow})$ interband transitions. This indicates that the position of the energy bands formed by

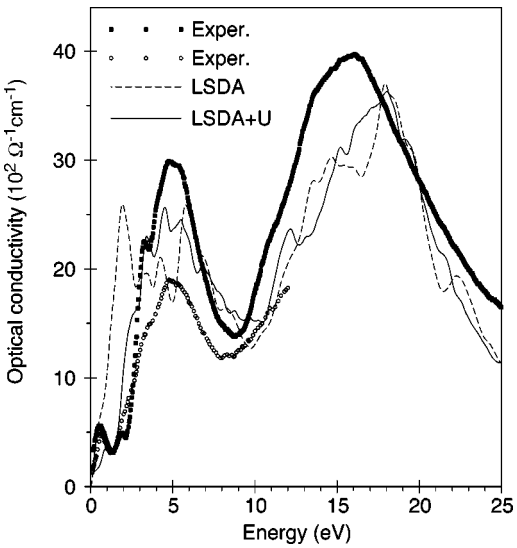

FIG. 6. The absorptive part of the diagonal optical conductivity of Fe_3O_4 calculated in LSDA (dashed line) and LSDA$+U$ (solid line) approximations compared with experimental data Ref. 24 (solid squares) and Ref. 23 (open circles).

$Fe_B^{2+}(e_{\downarrow})$ states are not reproduced very well in the LSDA $+U$ calculations. One of the possible reasons for this is the use in our calculations of the ideal inverse spinel structure without any distortion with equal O^{2-}-Fe_B^{2+} and O^{2-}-Fe_B^{3+} distances. In reality one should expect a shift of the oxygen ions towards Fe_B^{3+} ions and outwards from the Fe_B^{2+} ions. The decrease of the O^{2-}-Fe_B^{2+} hybridization due to the increase of the distance between them would lead to weaker bonding-antibonding splitting of the $Fe_B^{2+}(e_{\downarrow})$ states (Fig. 3). As a result peak 3 would be shifted towards larger energies. We have not calculated the electronic structure of the distorted Fe_3O_4 because just how the displacements of the at-

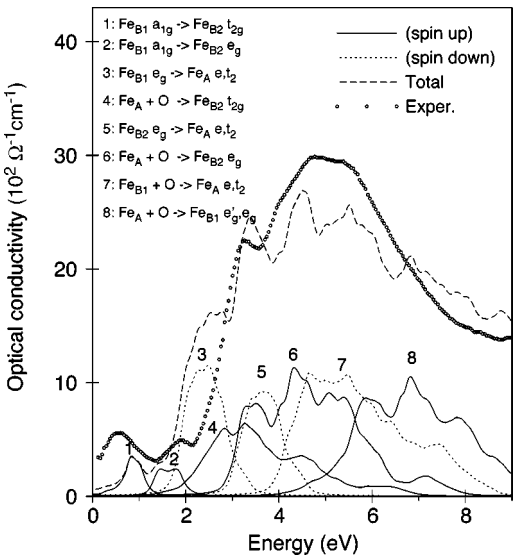

FIG. 7. Contributions of different interband transitions to the absorptive part of the diagonal optical conductivity of Fe_3O_4 compared with experimental data (Ref. 24) (open circles).

oms arrange themselves has been the subject of debate for a long time and still is a controversial problem (see Refs. 62, 63 and references therein).

Let us consider now the magneto-optical properties of Fe_3O_4. In the polar geometry, where the z -axis is chosen to be perpendicular to the solid surface, and parallel to the magnetization direction, the expression for small Kerr angles is given by[64]

$$\theta_K + i\epsilon_K = \frac{\varepsilon_{xy}}{(1-\varepsilon_{xx})\sqrt{\varepsilon_{xx}}} \tag{1}$$

with θ_K and ϵ_K being the Kerr rotation and Kerr elipticity, respectively. $\varepsilon_{\alpha\beta}(\alpha,\beta \equiv x,y,z)$ is the dielectric tensor, which is related to the optical conductivity tensor $\sigma_{\alpha\beta}$ through

$$\varepsilon_{\alpha\beta}(\omega) = \delta_{\alpha\beta} + \frac{4\pi i}{\omega}\sigma_{\alpha\beta}(\omega). \tag{2}$$

In Fig. 8 we show the experimentally measured[28] Kerr rotation $\theta_K(\omega)$ and Kerr elipticity $\epsilon_K(\omega)$MO spectra of Fe_3O_4, as well as the off-diagonal parts of the dielectric function calculated with the LSDA and LSDA$+U$ approximations. This picture clearly demonstrates that the better description is achieved with the LSDA$+U$ approach.

We mention that although the O $2p \rightarrow$ Fe $3d$ interband transitions, which start already from about 2.5 eV (see Fig. 7), play an important role in the formation of the optical spectra of Fe_3O_4, the Kerr spectra are mostly determined by transitions between energy bands which have predominantly Fe $3d$ character. The reason for this is that the spin-orbit and exchange splitting of O $2p$ states is much smaller in comparison with the Fe $3d$ ones. The minimum in the Kerr rotation spectrum at 0.9 eV is due to the $Fe_B^{2+}(a_{1g\uparrow}) \rightarrow Fe_B^{3+}(t_{2g\uparrow})$ interband transitions. The second maximum at about 2 eV is associated with the $Fe_B^{2+}(a_{1g\uparrow}) \rightarrow Fe_B^{3+}(e_{g\uparrow})$ interband transitions. The minimum in the Kerr rotation spectrum between 3 and 4 eV can be associated with the $Fe_B^{3+}(e_{g\downarrow}) \rightarrow Fe_A^{3+}(e_{\downarrow}, t_{2\downarrow})$ transitions. In conclusion, we should mention that at least below 2 eV our LSDA$+U$ band-structure calculations support the assignment of the MO-active transitions in Fe_3O_4 drawn earlier in Ref. 26 on the basis of the experimental data.

We should note that all the experimental measurements of the Kerr spectra of Fe_3O_4 (Refs. [25–28]) have been performed at *room temperature*. The LSDA$+U$ calculations, in comparison with the LSDA ones, describe better the electronic structure, optical, and MO properties not only in the low-temperature semiconducting phase but also in the high-temperature metallic phase of Fe_3O_4. This leads to a conclusion that Fe d electrons remain ''correlated'' above T_V. The main effect of heating through T_V is a disappearance of the long-range charge order on the B sublattice. This leads to the rearrangement of the electronic states in a small vicinity of the Fermi level and to the closing of the energy gap. However, high-energy Hubbard bands, whose energy position is mainly determined by on-site exchange and correlation interactions, remain almost unaffected ($U_{\text{eff}} \sim 4$–5 eV is much larger than $T_V \sim 0.01$ eV). This picture is supported by recent optical measurements,[24] which show a strong temperature dependence of the optical properties of Fe_3O_4 only in the range from 0 to 1 eV. The absolute value of the measured prominent peak in the optical absorption for photon energies around 0.6 eV determined by the $Fe_B^{2+}(a_{1g\uparrow}) \rightarrow Fe_B^{3+}(t_{2g\uparrow})$ interband transitions (Fig. 7) gradually decreases by about 30% when changing the temperature from 10 to 490 K. However, the other parts of the spectrum change very little. Further evidence can be found from the temperature-dependent magnetic circular dichroism (MCD) measurements of Fe_3O_4.[31] MCD spectra in core-level absorption are element specific and site selective, thus providing valuable information on the energy position of empty states in a wide energy interval. It was found that the $M_{2,3}$MCD spectra of

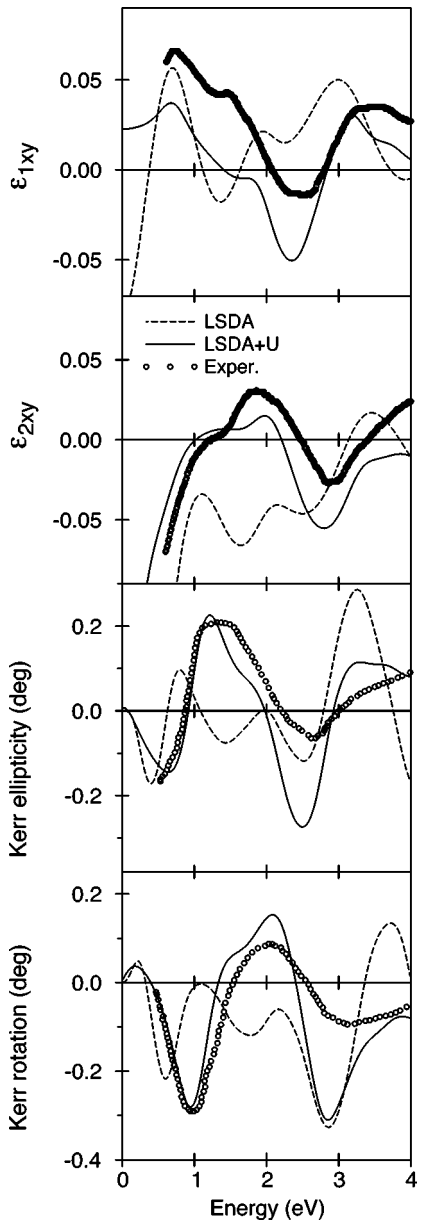

FIG. 8. Calculated off-diagonal parts of the dielectric function ε_{xy}, Kerr rotation, and Kerr ellipticity spectra of Fe_3O_4 compared with experimental data (circles) (Ref. 28).

Fe_3O_4 reflecting the Fe $3d$ unoccupied states are almost identical for 50 and 300 K.

B. Mg^{2+} and Al^{3+} substituted Fe_3O_4

Nonmagnetic Al^{3+} ions can substitute Fe^{3+} ions both at the A and B sites. However, Mössbauer studies of relatively broad compositional range for the spinel system $Fe_{3-x}Al_xO_4$ indicate that Al up to $x=1.2$ shows a strong preference for octahedral B sites.[65] The optical and MO spectra of Al^{3+} substituted magnetite $Fe_A^{3+}[Fe^{2+}Fe_{1-x}^{3+}Al_x^{3+}]_BO_4^{2-}$ have been recently presented in Ref. 26 for $x=0.02$, 0.2, and 0.4.

The optical and MO spectra of Mg^{2+} substituted magnetite have been measured in Ref. 25. Unfortunately it was not possible to prepare the samples with substituted Mg^{2+} ions only at octahedral B sites. Mg^{2+} ions occupy both the octahedral B and tetrahedral A sites. The cation distribution formula for substituted magnesium is $[Mg_x^{2+}Fe_{1-x}^{3+}]_A[Mg_{1-x}^{2+}Fe_{1+x}^{3+}]_BO_4^{2-}$ with $x=0.1$, 0.13, and 0.24.[25] The optical measurements clearly show that Mg substituted magnetite is a semiconductor with a substantially larger gap in comparison with pure magnetite.[25] $Fe_A^{3+}[Mg^{2+}Fe^{3+}]_BO_4^{2-}$ is already a charge ordered compound with Mg^{2+} and Fe^{3+} ions occupying $B1$ and $B2$ sites, respectively. The infrared reflectivity measurements on Mg substituted magnetite at 10 K performed in Ref. 25 show that the spectrum is nearly identical to the room-temperature data.

We have calculated the electronic structure, optical, and MO properties of both the magnesium and aluminum substituted magnetite using the LSDA and LSDA$+U$ approximations. The local symmetry in substituted magnetite is reduced to C_{2v} and C_{2h} at the A and B sites, respectively. The crystal field causes the d orbitals to split into five singlets at each site: a_1', a_1'', b_1, a_2, and b_2 at the A site and a_{g1}, a_{g2}, a_{g3}, b_{g1}, and b_{g2} at the B site. The tetrahedral component of the crystal field at the A site is strong enough that the a_1'', a_2 ($3z^2-1$ and x^2-y^2) and a_1', b_1, and b_2 (the linear combination of the xy, yz, and xz) orbitals form two separate nonoverlapping bands. However, the $a_1''-a_2$ and $a_1'-b_1-b_2$ splitting is negligible in comparison with their widths, therefore we present in Figs. 9 and 12 DOS of e orbitals as a sum of the a_1'' and a_2 orbitals and t_2 as a sum of the a_1', b_1, and b_2 ones. Correspondingly, at the octahedral B site we sum the DOS of a_{g3} and b_{g2} (former e_g) and a_{g1}, a_{g2}, and b_{g1} (former t_{2g} orbitals).

Figure 9 shows the LSDA$+U$ partial density of states of magnesium substituted magnetite $Fe_A^{3+}[Mg^{2+}Fe^{3+}]_BO_4^{2-}$. The energy-band structure is very similar to the band structure of pure magnetite (compare Figs. 9 and 4), except that there are no Fe_B^{2+} states in the magnesium substituted magnetite. Because the occupied Fe_B^{2+} $a_{1g\uparrow}$ and $e_{g\downarrow}'$ states of Fe_3O_4, situated in the vicinity of the Fermi level just drop out in the Mg_B^{2+} substituted magnetite the Fermi level in the latter compound is placed at the top of the oxygen $2p$ bands.

Although the LSDA calculations are able to predict the correct insulating ground state of Mg_B^{2+} substituted magnetite, they significantly underestimate the energy gap and give a wrong energy position for the d states. As a consequence, the LSDA calculations give unsatisfactory agreement between calculated and experimental optical spectra in the 0–3-eV energy interval (Fig. 10). The LSDA$+U$ calculations produce a larger energy gap, shift the energy bands from the vicinity of the Fermi level, and, as a result, give a substantial improvement over the LSDA results (Fig. 10). As we mentioned above, below 2.5 eV the optical spectra of pure magnetite are determined only by interband transitions between Fe $3d$ bands. It is not the case for Mg_B^{2+} substituted magnetite. It was found that for the substituted compound strongly hybridized Mg $3p$ and O $2p$ states situated just under the Fermi level (Fig. 9) determine the optical spectra. In particular, the prominent peaks of the optical conductivity and ε_{xx} at 3.5 eV are determined by the O $(2p_\downarrow) \rightarrow Fe_A^{3+}(e_\downarrow, t_\downarrow)$ and O $(2p_\uparrow) \rightarrow Fe_B^{3+}(e_{g\uparrow}, t_{2g\uparrow})$ interband transitions.

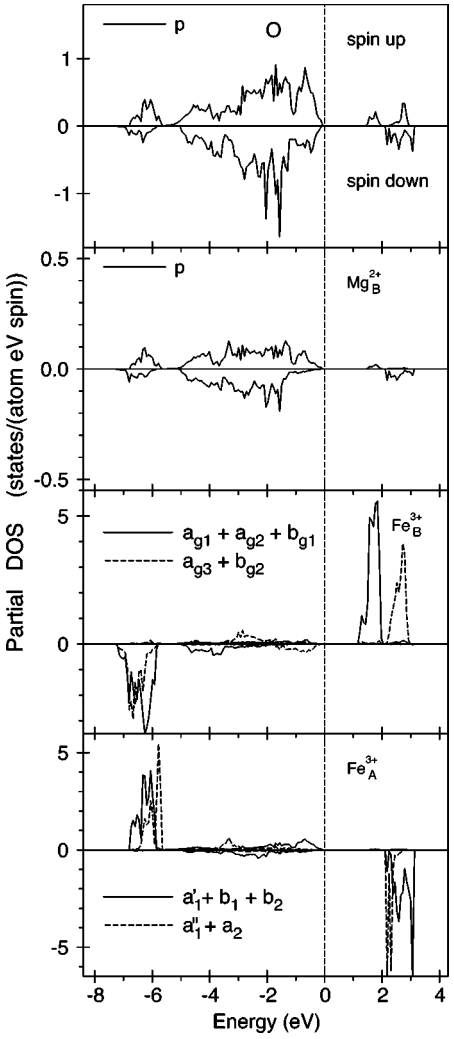

FIG. 9. LSDA$+U$ partial DOS of Mg_B^{2+} substituted magnetite.

After consideration of the band structure and optical properties we turn to the magneto-optical spectra. Compared to pure magnetite the MO spectra of Mg_B^{2+} substituted magnetite show a decrease of the negative Kerr rotation near 0.9 eV by a factor of approximately 10.[25] Also the rest of the spectra

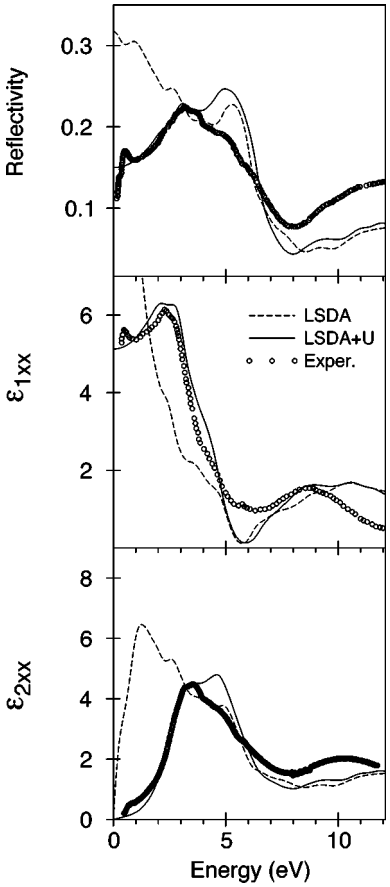

FIG. 10. Optical reflectivity and diagonal parts of the dielectric function ε_{xx} of Mg_B^{2+} substituted magnetite calculated within LSDA (dashed line) and LSDA$+U$ (solid line) approximations compared with experimental data (Ref. 23) (circles).

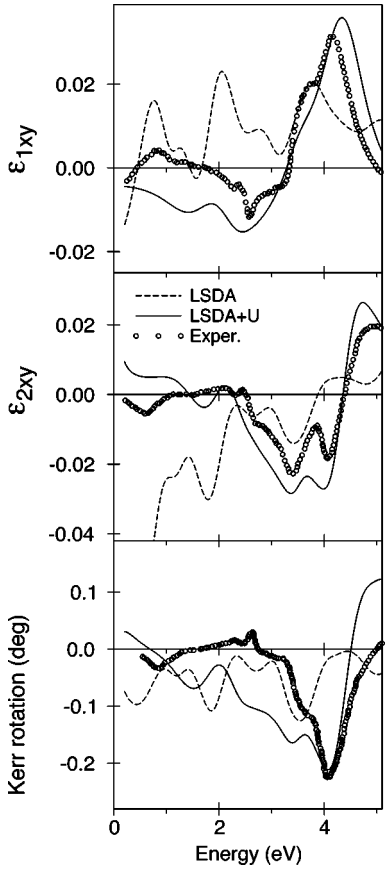

FIG. 11. The off-diagonal parts of the dielectric function ε_{xy} and the Kerr rotation spectrum for Mg_B^{2+} substituted magnetite calculated within LSDA (dashed line) and LSDA$+U$ (solid line) approximations compared with experimental data (Ref. 25) (circles) for $[Mg_{0.1}^{2+}Fe_{0.9}^{3+}]_A[Mg_{0.9}^{2+}Fe_{01}^{2+}Fe_{1.0}^{3+}]_BO_{3.95}^{2-}$.

differ markedly from those of pure magnetite. The best agreement between theory and experiment for the MO spectra was found to be when we used the LSDA$+U$ approximation. In Fig. 11 we show the experimentally measured[25] Kerr rotation spectrum of Mg_B^{2+} substituted magnetite, as well as off-diagonal parts of the dielectric function calculated with the LSDA and LSDA$+U$ approximations. The Fe_B^{2+} $a_{1g\uparrow}$ states, responsible for the prominent minimum in Kerr rotation spectrum around 0.9 eV in pure magnetite, do not exist any more. Therefore this fine structure disappears in the MO spectrum of Mg_B^{2+} substituted magnetite.

The experimental features of the Kerr rotation and off-diagonal optical conductivity spectra are reasonably well reproduced by the LSDA$+U$ calculations. However, the theory predicts larger Kerr rotation in the 1.5–3.5 eV energy interval. One of the possible reasons of such disagreement might be the following. Our theoretical calculations were performed for the ideally substituted magnetite $Fe_A^{3+}[Mg^{2+}Fe^{3+}]_BO_4$. On the other hand, the experimentally measured magnesium magnetite had the nominal composition $[Mg_{0.1}^{2+}Fe_{0.9}^{3+}]_A[Mg_{0.9}^{2+}Fe_{0.1}^{2+}Fe_{1.0}^{3+}]_BO_4$. In Fe_3O_4 the magnetic moments within the A and B sublattices are ferromagnetically aligned while the two sublattices are antiferromagnetic with respect to each other, therefore the Kerr rotation spectrum is composed by the signals coming from the A and B sublattices with opposite signs. Even a small deviation from the ideally substituted magnetite can greatly affect the compensation effect between the A and B sublattices in the Kerr rotation spectrum.

The LSDA$+U$ band structure of Al_B^{3+} substituted Fe_3O_4 is also very similar to the band structure of pure magnetite (compare Figs. 12 and 4), except that in the aluminum substituted magnetite there are no Fe_B^{3+} energy bands. They simply drop out in the Al_B^{3+} substituted magnetite with very little change in the position and widths of the rest of the energy bands.

In Fig. 13 we show the experimentally measured[26] Kerr rotation $\theta_K(\omega)$ spectrum as well as off-diagonal parts of the dielectric function of aluminum substituted magnetite with the nominal composition $Fe_A^{3+}[Fe^{2+}Fe_{0.6}^{3+}Al_{0.4}^{3+}]_BO_4$ in comparison with the LSDA$+U$ calculated spectra for the ideally substituted $Fe_A^{3+}[Fe^{2+}Al^{3+}]_BO_4$ compound. As the prominent minimum at 0.9 eV in the Kerr rotation spectrum of Fe_3O_4 is completely determined by the interband transitions between d states of Fe_B^{2+} and Fe_B^{3+} ions it should be suppressed if either initial (Fe_B^{2+} d) or final (Fe_B^{3+} d) bands for these transitions disappear from the band structure upon substitution. The first case is realized in Mg substituted magne-

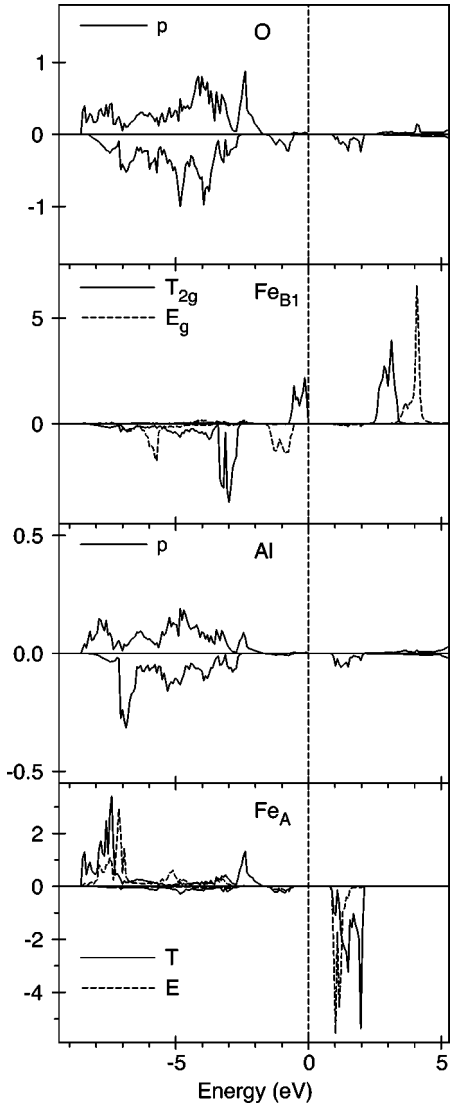

FIG. 12. LSDA+U partial DOS of Al_B^{3+} substituted magnetite.

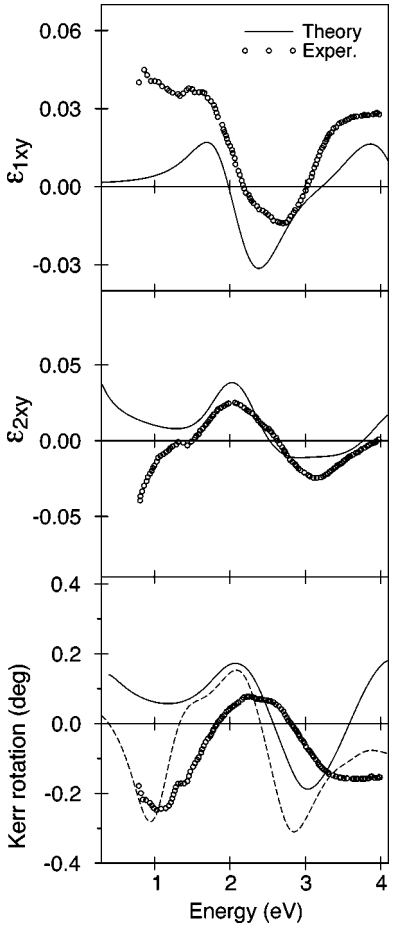

FIG. 13. Calculated off-diagonal parts of the dielectric function ε_{xy} and the Kerr rotation spectrum for Al^{3+} substituted magnetite (full line) compared with experimental data (circles) for $Fe_A^{3+}[Fe^{2+}Fe_{1-x}^{3+}Al_x^{3+}]_BO_4^{2-}$ ($x=0.4$) compound (Ref. 26); dashed line shows theoretically calculated Kerr rotation spectrum of Fe_3O_4.

tite (see Fig. 11). In Al substituted magnetite, on the other hand, Fe_B^{3+} ions are replaced by Al^{3+}. There are no Fe_B^{3+} derived d bands above the Fermi level and, as a result, the calculated Kerr rotation remains positive below 2 eV. In contrast to the calculations, the measurements of the Kerr rotation spectra have been performed for partially substituted compound in which only 40% of Fe_B^{3+} ions were replaced by Al. Therefore the minimum at about 1.0 eV derived from the transitions to Fe_B^{3+} states is still present in the experimental spectrum (Fig. 13), however, its magnitude is smaller than in pure magnetite. Experimental measurements of the Kerr rotation spectrum of completely substituted $AlFe_2O_4$ are highly desired.

IV. SUMMARY

In contrast to LSDA, where the stable solution is a metal with a uniform distribution of the $t_{2g\uparrow}$ electrons on the octahedral sites, the LSDA+U gives a charge-ordered insulator with the direct energy gap of 0.19 eV. However, in our band-structure calculations we regard the Fe_3O_4 compound as an ideal system with perfect charge ordering with $b1$ chains occupied only by Fe^{2+} ions and $b2$ chains by Fe^{3+} ions (the Verwey type of ordering[2]). The real situation is much more complicated. As shown in Ref. 16 above T_V magnetite becomes metallic, but with a very small value of the density of states at the Fermi level, which becomes larger with increasing temperature. Another temperature-dependent photoemission measurement[22] shows that on heating through the transition temperature T_V the single-particle gap is not eliminated immediately, but gradually reduces with the increasing of temperature above the Verwey transition. This can be an indication of the existence of a short-range charge order or many different short-range charge ordered states with frustrated geometries above T_V, as proposed by Anderson.[35] Such states are gradually lost on increasing the temperature. We also note that the charge order below T_V is more complicated than the simple Verwey pattern, and that the phase transition is accompanied by a structural transformation from cubic spinel to monoclinic structure.[40,41]

The LSDA+U calculations give reasonably good agreement between theoretically calculated and experimentally

measured optical and MO spectra of Fe_3O_4. The minimum in the Kerr rotation spectrum at 0.9 eV is due to the $Fe_B^{2+}(a_{1g\uparrow}) \rightarrow Fe_B^{3+}(t_{2g\uparrow})$ interband transitions. The second maximum at about 2 eV is associated with the $Fe_B^{2+}(a_{1g\uparrow}) \rightarrow Fe_B^{3+}(e_{g\uparrow})$ interband transitions. The minimum in the Kerr rotation spectrum between 3 and 4 eV can be associated with the $Fe_B^{3+}(e_{g\downarrow}) \rightarrow Fe_A^{3+}(e_\downarrow, t_{g\downarrow})$ interband transitions. In general, our LSDA+U band-structure calculations support the picture of the MO-active transitions in Fe_3O_4 drawn earlier by Fontijn *et al.*[26] using the experimental data.

Although the LSDA calculations were able to predict the correct insulating ground state of Mg_B^{2+} substituted magnetite, they significantly underestimate the energy gap and give a wrong energy position for the *d* states. As a consequence, the LSDA calculations give unsatisfactory agreement between calculated and experimental optical and MO spectra in the 0–3 eV energy interval. LSDA+U calculations produce a larger energy gap, shift the energy bands from the vicinity of the Fermi level and as a result give a substantial improvement over the LSDA results.

Finally, we would like to point out that while the LSDA +U approach does a better job than the LSDA in the treatment of correlation effects, it is still unclear how well it performs in evaluating the subtle energies and interactions affecting the charge ordered ground state and the higher temperature short-range ordered states. Magnetite is likely to remain scientifically interesting for many more years as befits its remarkable history.

ACKNOWLEDGMENTS

This work was carried out at the Ames Laboratory, which is operated for the U.S. Department of Energy by Iowa State University under Contract No. W-7405-82. This work was supported by the Director for Energy Research, Office of Basic Energy Sciences of the U.S. Department of Energy. V. N. Antonov gratefully acknowledges the hospitality during his stay at Ames Laboratory.

*Permanent address: Institute of Metal Physics, 36 Vernadskii str., 252142 Kiev, Ukraine.

[1] N. F. Mott, Proc. R. Soc. London, Ser. A **62**, 416 (1949); Adv. Phys. **16**, 49 (1967); Can. J. Phys. **34**, 1356 (1956); Philos. Mag. **6**, 287 (1961).

[2] E. J. Verwey and P. Haaỳman, Physica (Amsterdam) **8**, 1979 (1941).

[3] J. Smit and H. P. J. Wijn, *Ferrites* (Philips Technical Library, Eindhoven, 1959).

[4] V. A. M. Brabers, in *Handbook of Magnetic Materials*, edited by K. H. J. Buschow (Elsevier Science, Amsterdam, 1995), Vol. 8, p. 199.

[5] *Electronic Conduction in Oxides*, edited by N. Tsuda, K. Nasu, A. Yansen, and K. Siratory, Springer Series in Solid State Science Vol. 94 (Springer-Verlag, Berlin, 1991); N. F. Mott, *Metal-Insulator Transitions* (Taylor and Francis, London, 1995); J. Zaanen, G. A. Sawatzky, and J. W. Allen, Phys. Rev. Lett. **55**, 418 (1985); H. Sawada and K. Terakura, Phys. Rev. B **58**, 6831 (1998); S. Kondo, D. C. Johnson, C. A. Swenson, F. Borsa, A. V. Mahajan, L. L. Miller, T. Gu, A. I. Goldman, M. B. Maple, D. A. Gajewski, E. J. Freeman, N. R. Dilley, R. P. Dickey, J. Merrin, K. Kojima, G. M. Luke, Y. J. Uemura, O. Chmaissem, and J. D. Jorgensen, Phys. Rev. Lett. **78**, 3729 (1997).

[6] N. F. Mott, Philos. Mag. B **42**, 327 (1980), and the articles in the same series.

[7] B. A. Calhoun, Phys. Rev. **94**, 1577 (1954); P. A. Miles, W. B. Westphal, and A. von Hippel, Rev. Mod. Phys. **29**, 279 (1957); M. Motsui, S. Todo, and S. Chikazumi, J. Phys. Soc. Jpn. **42**, 1517 (1977).

[8] E. J. Verwey, P. Haayman, and F. Romrin, J. Chem. Phys. **15**, 181 (1947).

[9] Y. Fujii, G. Shirane, and Y. Yamada, Phys. Rev. B **11**, 2036 (1975).

[10] M. Iizumi and G. Shirane, Solid State Commun. **17**, 433 (1975).

[11] S. Iida, K. Mizushima, M. Mada, J. Umemura, and J. Yoshida, J. Appl. Phys. **49**, 1455 (1978).

[12] R. J. Lad and V. E. Henrich, Phys. Rev. B **39**, 13 478 (1989).

[13] Y. Ma, P. D. Johnson, N. Wassdahl, J. Guo, P. Skytt, J. Nordgren, S. D. Keven, J. E. Rubensson, T. Böske, and W. Eberhardt, Phys. Rev. B **48**, 2109 (1993).

[14] S. G. Bishop and P. C. Kemeny, Solid State Commun. **15**, 1877 (1974).

[15] A. J. M. Kuipers and V. A. M. Brabers, Phys. Rev. B **14**, 1401 (1976); Phys. Rev. B **20**, 594 (1979).

[16] A. Chainani, T. Yokoya, T. Morimoto, T. Takahashi, and S. Todo, Phys. Rev. B **51**, 17 976 (1995).

[17] S. F. Alvarado, W. Eib, F. Meier, D. T. Pierce, K. Sattler, H. C. Siegmann, and J. P. Remeika, Phys. Rev. Lett. **34**, 319 (1975); S. F. Alvarado, M. Erbudak, and P. Munz, Phys. Rev. B **14**, 2740 (1976).

[18] K. Siratory, S. Suga, M. Taniguchi, K. Soda, S. Kimura, and A. Yanase, J. Phys. Soc. Jpn. **55**, 690 (1986).

[19] T. Schedel-Niedring, W. Weiss, and R. Schlögl, Phys. Rev. B **52**, 17 449 (1995).

[20] M. Sancrotti, F. Ciccacci, M. Finazzi, E. Vescovo, and S. F. Alvarado, Z. Phys. B: Condens. Matter **84**, 243 (1991).

[21] Y. Q. Cai, M. Ritter, W. Weis, and A. M. Bradshaw, Phys. Rev. B **58**, 5043 (1998).

[22] J. H. Park, L. H. Tjeng, J. W. Allen, P. Metcalf, and C. T. Chen, Phys. Rev. B **55**, 12 813 (1997).

[23] A. Schlegel, S. F. Alvarado, and P. Wachter, J. Phys. C **12**, 1157 (1979).

[24] S. K. Park, T. Ishikawa, and Y. Tokura, Phys. Rev. B **58**, 3717 (1998).

[25] X. Zhang, J. Schoenes, W. Reim, and P. Wachter, J. Phys. C **16**, 6055 (1983).

[26] W. F. J. Fontijn, P. J. van der Zaag, M. A. C. Deviller, V. A. M. Brabers, and R. Metselaar, Phys. Rev. B **56**, 5432 (1997).

[27] Z. Simsa, H. LeGall, and P. Siroky, Phys. Status Solidi B **100**, 666 (1980); Z. Simsa, P. Siroky, J. Kolacek, and V. A. Brabers, J. Magn. Magn. Mater. **15-18**, 775 (1980).

[28] X. Zhang, J. Schoenes, and P. Wachter, Solid State Commun. **39**, 189 (1981).

[29] S. Visnovsky, V. Prosser, R. Krishnan, V. Parizek, K. Nitsch, and L. Svobodova, IEEE Trans. Magn. **MAG-17**, 3205 (1981).

[30] P. Kuiper, B. G. Searle, L. C. Duda, R. M. Wolf, and P. J. van der Zaag, J. Electron Spectrosc. Relat. Phenom. **86**, 107 (1977).
[31] T. Koide, T. Shidara, K. Yamaguchi, A. Fujimori, H. Fukutani, N. Kimizuka, and S. Kimura, J. Electron Spectrosc. Relat. Phenom. **78**, 275 (1996).
[32] A. Yanase and K. Siratory, J. Phys. Soc. Jpn. **53**, 312 (1984).
[33] Z. Zhang and S. Satpathy, Phys. Rev. B **44**, 13 319 (1991).
[34] V. I. Anisimov, I. S. Elfimov, N. Hamada, and K. Terakura, Phys. Rev. B **54**, 4387 (1996).
[35] P. W. Anderson, Phys. Rev. **102**, 1008 (1956).
[36] J. R. Cullen, Solid State Commun. **13**, 1783 (1973); J. R. Cullen and E. R. Callen, Phys. Rev. Lett. **26**, 236 (1971); J. R. Cullen and E. R. Callen, Phys. Rev. B **7**, 397 (1973).
[37] N. F. Mott, Philos. Mag. **34**, 643 (1976); Adv. Phys. **16**, 49 (1967); Festkoerperprobleme **19**, 331 (1979).
[38] B. K. Chacraverty, Solid State Commun. **15**, 1271 (1974).
[39] M. Mizoguchi, J. Phys. Soc. Jpn. **44**, 1501 (1978); **44**, 1512 (1978).
[40] J. Yoshida and S. Iida, J. Phys. Soc. Jpn. **42**, 236 (1977).
[41] E. J. Samuelsen, E. J. Bleeker, L. Dobrzynski, and T. Riste, J. Appl. Phys. **39**, 1114 (1968).
[42] P. Villars and L. D. Calvert, *Pearson's Handbook of Crystallographic Data for Intermetallic Phases* (ASM International, Materials Park, OH, 1991).
[43] V. N. Antonov, V. P. Antropov, B. N. Harmon, A. Ya. Perlov, and A. N. Yaresko, Phys. Rev. B **59**, 14 552 (1999).
[44] V. N. Antonov, B. N. Harmon, A. Ya. Perlov, and A. N. Yaresko, Phys. Rev. B **59**, 14 561 (1999).
[45] U. von Barth and L. A. Hedin, J. Phys. C **5**, 1692 (1972).
[46] O. K. Andersen, Phys. Rev. B **12**, 3060 (1975); D. D. Koelling and B. N. Harmon, J. Phys. C **10**, 3107 (1977).
[47] V. V. Nemoshkalenko, A. E. Krasovskii, V. N. Antonov, Vl. N. Antonov, U. Fleck, H. Wonn, and P. Ziesche, Phys. Status Solidi B **120**, 283 (1983).
[48] V. N. Antonov, A. Ya. Perlov, A. P. Shpak, and A. N. Yaresko, J. Magn. Magn. Mater. **146**, 205 (1995).
[49] H. Ebert, Phys. Rev. B **38**, 9390 (1988).
[50] V. V. Nemoshkalenko and V. N. Antonov, *Computational Methods in Solid State Physics* (Gordon and Breach, London, 1998).
[51] V. N. Antonov, A. I. Bagljuk, A. Ya. Perlov, V. V. Nemoshkalenko, Vl. N. Antonov, O. K. Andersen, and O. Jepsen, Low Temp. Phys. **19**, 494 (1993).
[52] P. E. Blöchl, O. Jepsen, and O. K. Andersen, Phys. Rev. B **49**, 16 223 (1994).
[53] V. I. Anisimov, J. Zaanen, and O. K. Andersen, Phys. Rev. B **44**, 943 (1991).
[54] L. Néel, Ann. Phys. (Leipzig) **3**, 137 (1948).
[55] C. G. Shull, F. O. Wollan, and W. C. Koehter, Phys. Rev. **84**, 912 (1951).
[56] V. C. Rakhecha and N. S. Satya Murthy, J. Phys. C **11**, 4389 (1978).
[57] J. F. Herbst and J. W. Wilkins, in *Handbook of the Physics and Chemistry of Rare Earths*, edited by K. A. Gschneidner, L. Eyring, and S. Hüfner (North-Holland, Amsterdam, 1987), Vol. 10, p. 321.
[58] P. H. Dederics, S. Blügel, R. Zeller, and H. Akai, Phys. Rev. Lett. **53**, 2512 (1984).
[59] V. I. Anisimov and O. Gunnarsson, Phys. Rev. B **43**, 7570 (1991).
[60] V. N. Antonov, A. N. Yaresko, A. Ya. Perlov, P. Thalmeier, P. Fulde, P. M. Oppeneer, and H. Eschrig, Phys. Rev. B **58**, 9752 (1998).
[61] J. M. Ziman, *Models of Disorder: The Theoretical Physics of Homogeneously Disordered Systems* (Cambridge University Press, Cambridge, England, 1979).
[62] Z. Kakol and J. M. Honig, Phys. Rev. B **40**, 9090 (1989).
[63] K. Siratory, Y. Ishii, Y. Morii, S. Funashi, S. Todo, and A. Yanase, J. Phys. Soc. Jpn. **67**, 2818 (1998).
[64] W. Reim and J. Schoenes, in *Ferromagnetic Materials*, edited by E. P. Wohlfarth and K. H. J. Buschow (North-Holland, Amsterdam, 1990), Vol. 5, p. 133.
[65] G. Dehe, B. Seidel, K. Melzer, and C. Michalk, Phys. Status Solidi A **31**, 439 (1975); G. Dehe, J. Suwalski, E. Weiser, and R. Kubisch, *ibid.* **65**, 669 (1981); M. Rosenberg, P. Deppe, H. U. Janssen, V. A. M. Brabers, F. S. Li, and S. Dey, J. Appl. Phys. **57**, 3740 (1985).